



tion force is extremely repulsive, the bosons exclude each other like fermions (i.e., the wave function vanishes where any two bosons meet), a phenomenon known as Bose–Fermi mapping or fermionization. In the opposite super-Tonks–Girardeau (sTG) limit [39–42] where the interaction is extremely attractive, there are excited states that can be mapped to the states at the TG limit.

Although the simplest system of two identical bosons has an analytical exact solution [43–46], the system of more particles lacks a general exact solution at arbitrary interaction strength. Various numerical approaches have been applied for approximate solutions [47–58]. Typically, these methods face the problem of balancing accuracy and feasibility. For instance, the correlated pair wave function (CPWF) [52] is a simple analytical function with nice accuracy. However, because it is fixed, it cannot correct its inherent deviation. The geometric wave function proposed in Ref. [54] is intrinsically an approximation, with several parameters determined numerically by the variational method to approach the exact solution. The direct diagonalization method [47] aims for accurate solutions but involves an enormous number of configurations and requires significant computational time, which may limit its accuracy and further calculations. Many of them restrict the interaction strength to a repulsive one, leaving room to investigate the attractive interaction and the sTG limit.

Compared with the ground state, fewer works have studied the excited eigenstates. Some of them [59–61] use group theory to study the energy spectra, especially their degeneracy at the limits of the interaction strength. Others use various numerical methods to calculate: multiconfiguration time-dependent Hartree method (MCTDH) combined with a relaxation technique [62]; physically transparent variational method [63, 64] obtaining the energy spectra; stochastic variational calculations [65]; effective interaction based on the two-particle relative harmonic-oscillator states [56]; and the GCM-CPWF [53] obtaining the first excited eigenstate. Among these studies, the first few eigenenergies and eigenstates are numerically obtained; however, the values and regularity of higher excited eigenstates at arbitrary interaction strength from numerical calculation remain unrevealed.

In this paper, by using the generator coordinate method (GCM), we study one of the prototypes lacking an exact solution — a gas of three identical bosons in a one-dimensional harmonic trap [60]. This case is significant not only as a stepping stone to more complex systems but also for its potential applications, such as creating anyons [66].

The (discretized) GCM [67–71] has been developed as an efficient approach to approximate solutions of quantum many-body problems. It does this by superposing the so-called generating functions while retaining collective properties. It has various adaptations in diverse fields [72–84], demonstrating great flexibility and power in

solving quantum many-body problems. The key to the GCM is selecting the appropriate form of generating functions [85, 86], which ensures good solution accuracy while maintaining a relatively small number of generating functions, thereby keeping computational costs low.

In Ref. [53], the GCM has been used with an analytical function CPWF [52] as the generating function to solve the system we are considering. Here, we use the GCM to solve this system but with a different generating function. We set it as a polynomial description multiplied by the system’s asymptotic function (polynomial ansatz, PA). This approach is inspired by a fundamental power series method for solving the single-particle harmonic oscillator [87] and independent of further assumptions of the wave function.

Our paper is organized as follows. In Section 2 we introduce the system and propose our GCM-PA method, detailing the analytical calculation of the GCM kernels. The results are presented in Section 3, including the eigenenergies spectra and eigenstate patterns, followed by some verifications and discussions. In Section 4 we mark a summary.

## 2 System and method

The system we consider is an ultracold one-dimensional gas of  $N = 3$  identical bosons with contact interaction, confined in a harmonic trap. The positions of these three bosons are denoted by  $(x_1, x_2, x_3)$ . The reduced Hamiltonian, expressed in dimensionless harmonic oscillator units  $\hbar = m = \omega = 1$ , is given by

$$\hat{H}_t = -\frac{1}{2} \sum_{i=1}^3 \frac{\partial^2}{\partial x_i^2} + \frac{1}{2} \sum_{i=1}^3 x_i^2 + g \sum_{1 \leq i < j \leq 3} \delta(x_i - x_j). \quad (2.1)$$

The contact interaction between each pair of bosons is described by a  $\delta$ -function with a uniform coupling strength  $g$ , where  $g > 0$  represents a repulsive interaction and  $g < 0$  an attractive one. The wave function must exhibit the BE exchange symmetry.

The nature of the harmonic oscillator allows us to separate the total (t) Hamiltonian into two parts: relative (r) and center-of-mass (c). The relative part depends only on the relative distance  $r_{ij} = |x_i - x_j|$  of each pair  $(i, j)$  of bosons, while the c.o.m. part only the normalized coordinate  $R = \frac{1}{\sqrt{3}} \sum_i x_i$ :

$$\hat{H}_r = -\frac{1}{6} \sum_{i < j} (\partial_{x_i} - \partial_{x_j})^2 + \frac{1}{6} \sum_{i < j} r_{ij}^2 + \sum_{i < j} g \delta(r_{ij}), \quad (2.2)$$

$$\hat{H}_c = \hat{H}_t - \hat{H}_r = -\frac{1}{2} \partial_R^2 + \frac{1}{2} R^2. \quad (2.3)$$



$\hat{H}_c$  is a simple Hamiltonian for a one-dimensional single-particle harmonic oscillator. Hereinafter, we will focus on the solution with positive parity of the relative Hamiltonian.

## 2.1 Polynomial ansatz

To discover the solution of the relative Hamiltonian, we start with the asymptotic properties at  $r_{ij} \rightarrow \infty$  due to the harmonic trap, which is a Gaussian function:

$$\Psi_{\mathbf{r}} \sim \exp\left(-\frac{1}{6} \sum_{i < j} r_{ij}^2\right) = G_{\mathbf{r}}. \quad (2.4)$$

We propose an ansatz where the remaining part of the wave function is described as a polynomial of the relative coordinates  $\{r_{ij}\}$ , determined by the interaction strength  $g$ :

$$\Psi_{\mathbf{r}}(\mathbf{r}) = p(g; r_{12}, r_{13}, r_{23})G_{\mathbf{r}}. \quad (2.5)$$

This is referred to as the polynomial ansatz (PA) hereinafter.

The analytical exact ground states at two limits of  $g$  are already known [9, 34] with their form consistent with the PA. In the BE condensation case  $g = 0$ , we have a trivial ground eigenfunction with an (unnormalized) polynomial part  $p = 1$  and corresponding eigenenergy  $E_{\mathbf{r}} = 1$ ; In the TG gas  $g \rightarrow +\infty$ , the ground eigenenergy is  $E_{\mathbf{r}} = 4$  and the corresponding  $p = \prod_{i < j} r_{ij} = r_{12}r_{13}r_{23}$  is the Vandermonde determinant [34, 88]. Generally,  $p$  may not be a polynomial with finite terms but a pseudo-polynomial; a truncation may serve as an approximation.

We apply the GCM to construct  $p(g; r_{12}, r_{13}, r_{23})$  by superposing the terms in the polynomial of  $\{r_{ij}\}$ , starting from the constant term and up to a truncating degree  $d$ . Due to the symmetry among  $r_{12}$ ,  $r_{13}$  and  $r_{23}$ , these terms can be symmetrized by the operator  $\hat{S}$  [87]. A generating function  $\phi$  then reads

$$\begin{aligned} \phi_{(n_3 n_2 n_1)}(r_{12}, r_{13}, r_{23}) &= \hat{S} r_{12}^{n_3} r_{13}^{n_2} r_{23}^{n_1} G_{\mathbf{r}} \\ (r_{ij} \geq 0; n_3 \geq n_2 \geq n_1 \geq 0) \end{aligned} \quad (2.6)$$

$\phi$  is normalized to  $\tilde{\phi}$  in advance to prevent the GCM kernel elements from blowing up as the polynomial degree  $n_3 + n_2 + n_1$  increases. The GCM wave function reads:

$$\Psi_{\text{GCM}} = \sum_{I=(n_3 n_2 n_1)}^{n_3+n_2+n_1 \leq d} c_I \tilde{\phi}_I. \quad (2.7)$$

We highlight the necessity of taking the absolute value  $r_{ij} = |x_i - x_j|$  in the generating function. This guarantees not only the BE statistics but also the Bethe–Peierls contact condition [10, 50, 89], which intro-

duces a discontinuity in the first-order derivative of the wave function, resulting in a  $\delta$ -term in the second order. Only then can the dynamic term cancel out the  $\delta$ -functional contact interaction in the Schrödinger equation. Any finite superposition of smooth functions will fail to represent the system properly because the required solution is outside the Hilbert space spanned by smooth functions.

## 2.2 GCM kernels

To obtain the weights  $c_I$  for each generating function  $\tilde{\phi}_I$  labeled by triplet  $I$  in the eigen-wave function, together with the eigenenergy  $E$ , one solves the Griffin–Hill–Wheeler (GHW) equation:

$$\mathcal{H}\mathbf{c} = E\mathcal{N}\mathbf{c}, \quad (2.8)$$

where  $\mathbf{c}$  is the vector of all the  $c_I$ , and  $\mathcal{N}$  and  $\mathcal{H}$ , the so-called normal kernel and Hamiltonian kernel, are defined as

$$\mathcal{N}_{IJ} = \langle \tilde{\phi}_I | \tilde{\phi}_J \rangle = \int \tilde{\phi}_I^\dagger(\mathbf{r}) \tilde{\phi}_J(\mathbf{r}) d\mathbf{r}, \quad (2.9)$$

$$\mathcal{H}_{IJ} = \langle \tilde{\phi}_I | \hat{H}_{\mathbf{r}} | \tilde{\phi}_J \rangle = \int \tilde{\phi}_I^\dagger(\mathbf{r}) \hat{H}_{\mathbf{r}} \tilde{\phi}_J(\mathbf{r}) d\mathbf{r}. \quad (2.10)$$

The GHW equation, which is a generalized eigenvalue equation of the two kernels, is solved following the procedure outlined in Ref. [71]. We neglect  $\mathcal{N}$ 's tiny eigenvalues, which are practically the ones less than the machine epsilon  $\epsilon = 10^{-12}$ . The ground and the first few eigenenergies, along with their corresponding eigenstates, are expected to be obtained in the GCM calculation.

To calculate the  $\mathcal{H}$  kernel, we expand the action of the Hamiltonian on a generating function  $\phi = pG_{\mathbf{r}}$  as

$$\begin{aligned} &\hat{H}_{\mathbf{r}} p(r_{12}, r_{13}, r_{23}) G_{\mathbf{r}} \\ &= G_{\mathbf{r}} \left[ p(r_{12}, r_{13}, r_{23}) - \sum_{\substack{k,l \neq j \\ 1 \leq k < l \leq 3 \\ 1 \leq j \leq 3}} \text{sgn}(x_j - x_k) \text{sgn}(x_j \right. \\ &\quad - x_l) \frac{\partial^2 p(r_{12}, r_{13}, r_{23})}{\partial r_{jk} \partial r_{jl}} + \sum_{1 \leq k < l \leq 3} r_{kl} \frac{\partial p(r_{12}, r_{13}, r_{23})}{\partial r_{kl}} \\ &\quad - \sum_{1 \leq k < l \leq 3} \frac{\partial^2 p(r_{12}, r_{13}, r_{23})}{\partial r_{kl}^2} - 2 \sum_{1 \leq k < l \leq 3} \delta(x_k \\ &\quad \left. - x_l) \frac{\partial p(r_{12}, r_{13}, r_{23})}{\partial r_{kl}} + gp(r_{12}, r_{13}, r_{23}) \sum_{1 \leq k < l \leq 3} \delta(x_k - x_l) \right]. \end{aligned} \quad (2.11)$$

The terms in Eq. (2.11) can be classified into those with the  $\delta$ -function (the last two terms in the square brackets), which arise from both the contact interaction and the dynamic term, and those without  $\delta$ -function. The  $\delta$ -term  $\delta(x_k - x_l)$  contributes only at the connection region  $x_k = x_l$ , while the non- $\delta$ -terms contribute over the region where  $x_1, x_2, x_3$  are different but have measure-zero contribution over the connection regions during the later

integration. Hence, for each specific relative magnitude relationship among  $x_1, x_2, x_3$ , the square bracket part to be integrated in Eq. (2.11) reduces to a polynomial.

To perform the integrations and later visualize the wave functions, it is convenient to transform the relative coordinates into orthonormal Jacobi coordinates  $X$  and  $Y$ :

$$\begin{cases} X = -\frac{1}{\sqrt{2}}(x_1 - x_2), \\ Y = -\frac{1}{\sqrt{6}}(x_1 + x_2) + \frac{2}{\sqrt{6}}x_3. \end{cases} \quad (2.12)$$

Thus, the relative magnitudes of  $x_1, x_2$ , and  $x_3$  divide the polar angle  $\theta = \arctan \frac{Y}{X}$  in the  $XY$ -plane into six equal parts (See Fig. 1). The wave functions of both each sextant and each dividing ray are symmetric due to the BE statistics, allowing us to integrate over only one sextant and one dividing ray.

The relative asymptotic Gaussian  $G_r$  transforms into the standard two-dimensional form  $\exp\left(-\frac{X^2+Y^2}{2}\right) = \exp\left(-\frac{\rho^2}{2}\right)$ . Consequently, the integrands in the two kernels  $\mathcal{H}$  and  $\mathcal{N}$  can be rewritten as the Gaussian  $G_r^2 = \exp(-\rho^2)$  multiplied by some polynomials of  $X = \rho \cos \theta$  and  $Y = \rho \sin \theta$ . The non- $\delta$ -part is integrated over  $\rho \in (0, +\infty)$  and  $\theta \in (\frac{\pi}{6}, \frac{\pi}{2})$  where  $x_1 < x_2 < x_3$ , while

$$\int_{x_1 < x_2 < x_3} X^a Y^b G_r^2 dX dY \Big|_{x_1 < x_2 < x_3} = \frac{1}{4} \Gamma\left(\frac{a+1}{2}\right) \Gamma\left(\frac{b+1}{2}\right) - 3^{-\frac{b+1}{2}} \frac{1}{2(b+1)} \Gamma\left(\frac{a+b+2}{2}\right) {}_2F_1\left(\frac{b+1}{2}, \frac{a+b+2}{2}, \frac{b+3}{2}, -\frac{1}{3}\right), \quad (2.13)$$

$$\int Y^b G_r^2 dY \Big|_{x_1 = x_2 < x_3} = \frac{1}{2} \Gamma\left(\frac{b}{2} + 1\right), \quad (2.14)$$

where  $\Gamma(a)$  is the gamma function and  ${}_2F_1(a, b, c, z)$  is the ordinary hypergeometric function [90]. All the results of elements in the kernels are algebraic numbers or elementary operations on  $\pi$ . Eventually, we obtain an analytical expression of our GCM kernels  $\mathcal{H}$  and  $\mathcal{N}$ , whose numerical values are used to solve the GHW equation.

The known properties at the limits  $g \rightarrow \pm\infty$ , such as fermionization and TG/sTG mapping, can be revealed in our GCM process. To see this, we isolate the  $\mathcal{H}_{\text{int}}$  part from the  $\mathcal{H}$  kernel, which is contributed by the contact interaction in the last term in Eq. (2.11) and arises only at the connection regions where  $r_{12}r_{13}r_{23} = 0$ . All the terms  $r_{12}^{n_3} r_{13}^{n_2} r_{23}^{n_1}$  where  $n_3, n_2, n_1 \geq 1$  vanish at these regions and annihilate their corresponding elements in the  $\mathcal{H}_{\text{int}}$  matrix, while the other elements (and thus in  $\mathcal{H}$ ) diverge when  $g \rightarrow \pm\infty$ . To ensure finite eigenenergies, the weights associated with the non-vanishing columns have to vanish, constraining the eigenstate to comprise only terms containing the factor  $r_{12}r_{13}r_{23}G_r$ , which vanish wherever  $r_{ij} = 0$ . This complete repulsion

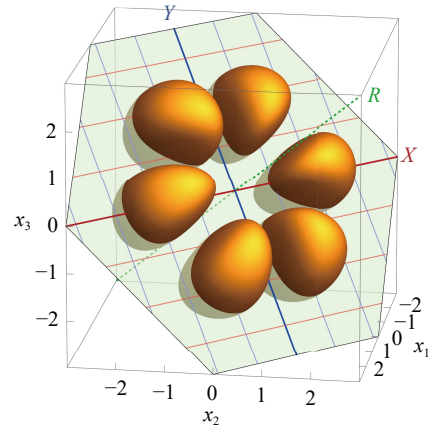


**Fig. 1** Illustration of the Jacobi coordinates ( $X, Y, R$ ) with the contour  $|\Psi_t|^2 = 0.1$  of a sample wave function  $\Psi_t = r_{12}r_{13}r_{23}G_t$  (which is the ground eigenstate at the TG limit). The gaps among the sextants of the wave function correspond to the connection regions  $x_1 = x_2$ ,  $x_1 = x_3$ , and  $x_2 = x_3$ .

the  $\delta$ -part in  $\mathcal{H}$  takes a specific  $\theta = \frac{\pi}{2}$  where  $x_1 = x_2 < x_3$ . These integrals can be analytically written as shown in Eqs. (2.13) and (2.14) for each single term in the integrand:

between bosons corresponds to the exclusion between identical fermions, known as the fermionization at the TG limit. The sign of  $g$ 's infinite value does not affect this result or the eigenstate, demonstrating the smooth connections between the finite TG and sTG solutions, known as the TG/sTG mapping.

### 3 Results and discussion

#### 3.1 Results and patterns

We applied the GCM-PA with a truncating polynomial degree  $d$  up to  $d = 18$ , where the dimension of independent generating functions is  $m = 62$ . Our process results in a regular series of eigenenergy and eigenstate spectra, as shown in Figs. 2 and 3. The eigenstates are labelled in a pair of numbers, which will be explained below. We display the relative eigenfunctions in the  $XY$ -plane with the Jacobi coordinates introduced above. The pattern is a cross-section of the 3-dimensional total state  $\Psi_t(\mathbf{x})$  by the plane  $x_1 + x_2 + x_3 = 0$  (see Fig. 1) and it exhibits  $C_{6v}$  symmetry due to the bosonic exchange symmetry.

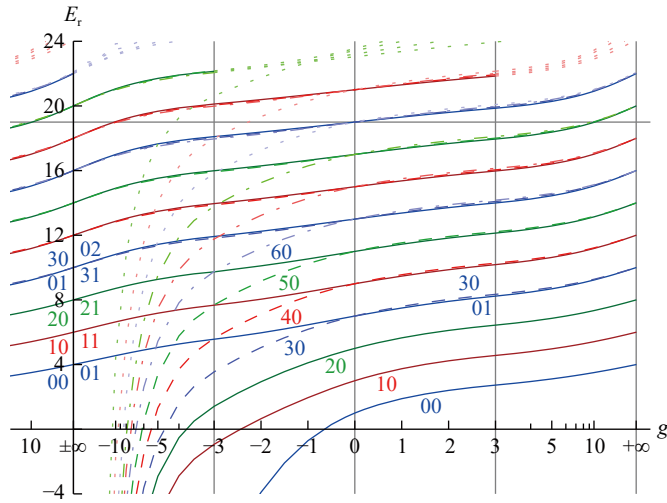


**Fig. 2** The relative eigenenergy spectra calculated by our GCM-PA with the truncating polynomial degree  $d = 18$ . On the  $g$  axis, the interval  $-3 \leq g \leq 3$  is linearly scaled, while  $|g| \geq 3$  uses a negative reverse scale. The limits  $g \rightarrow +\infty$  and  $g \rightarrow -\infty$  are connected, forming a barber pole-like loop. The grid line at  $E = 19 = d + 1$  corresponds to an upper limit of our calculation and spectra above  $E \approx 22$  are drawn dotted due to their apparent deviation.

In the ground state at attraction  $g < 0$ , the density concentrates around the regions where the bosons meet, particularly at the origin where all three bosons come together. As the attraction strength increases to infinity ( $g \rightarrow -\infty$ , the sTG limit), the ground eigenenergy drops to  $-\infty$ . At the BE limit  $g = 0$ , the relative ground eigenenergy is  $E_r = 1$ , and the corresponding eigenstate takes the form of a Gaussian function with  $SO(2)$  symmetry on the  $XY$ -plane. When the interaction becomes repulsive ( $g > 0$ ), gaps appear from the connection regions  $x_i = x_j$ , particularly at the origin. At the TG limit ( $g \rightarrow +\infty$ ), the relative ground eigenenergy is  $E_r = 4$  and the wave function at the connection regions vanishes. The reproduction of the BE and TG ground wave functions is verified by examining the solution weights on each polynomial.

The first two excited eigenstates, labeled as  $\Psi_{10}$  and  $\Psi_{20}$  in this work, exhibit similar evolution in the radial direction, gaining 1 and 2 additional nodes, respectively. The relative eigenenergies  $E_{10}$  and  $E_{20}$  increase with  $g$ , starting from  $E_r = 3$  and  $E_r = 5$  at the BE limit and reaching  $E_r = 6$  and  $E_r = 8$  at the TG limit, respectively.

Above the three lowest eigenstates, degeneracy and intersections occur in the spectra. In Figs. 2 and 3, the spectral lines are categorized into blue, red, and green series based on their degeneracies, and the degenerate spectra are distinguished by the shade of color and the solid/dashed/dotted type. In Fig. 2, below  $E \approx 22$ , both the color and the type are to mark the label  $i$  in the spectrum  $E_{ij}$ . Spectra  $E_{ij}$  sharing the same  $j$  are

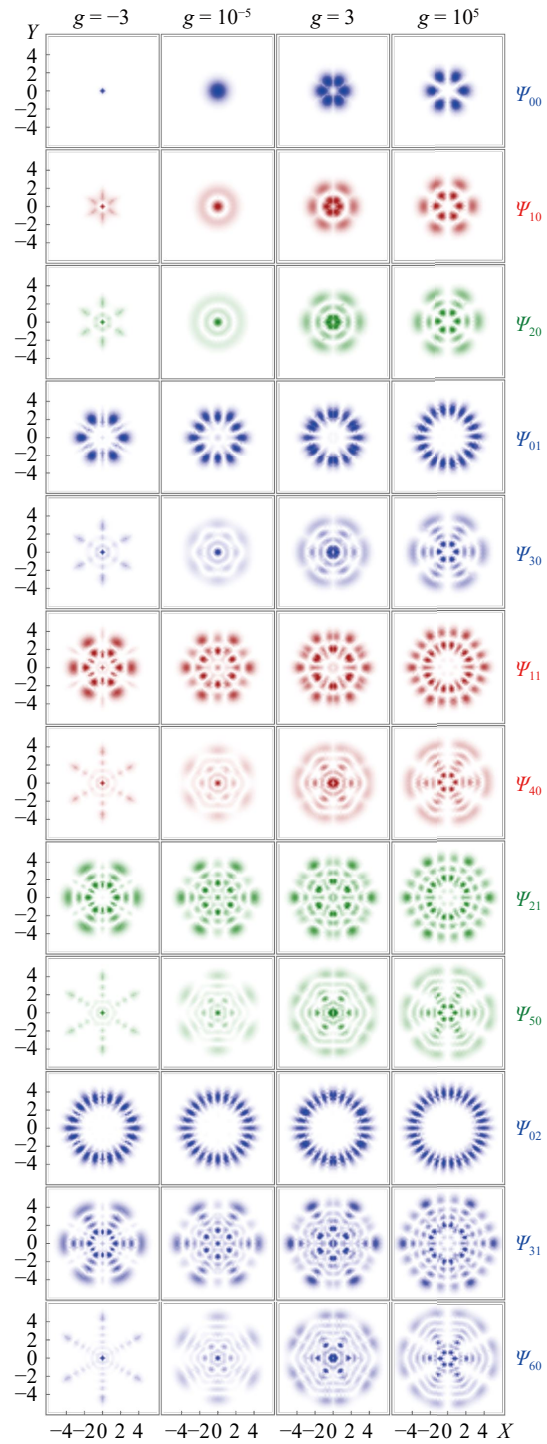


**Fig. 3** Evolution according to  $g$  of densities  $|\Psi(g)|^2$  of the first few eigenstates drawn in the  $XY$ -plane. The white color represents zero density. Neighboring states presented in the same color degenerate at the BE and TG limits. The  $g$  values are chosen nuance away from exact 0 and  $+\infty$  to separate the eigenstate patterns.

smoothly connected at the TG/sTG limit, forming a periodic structure, and are drawn in the same color and type.

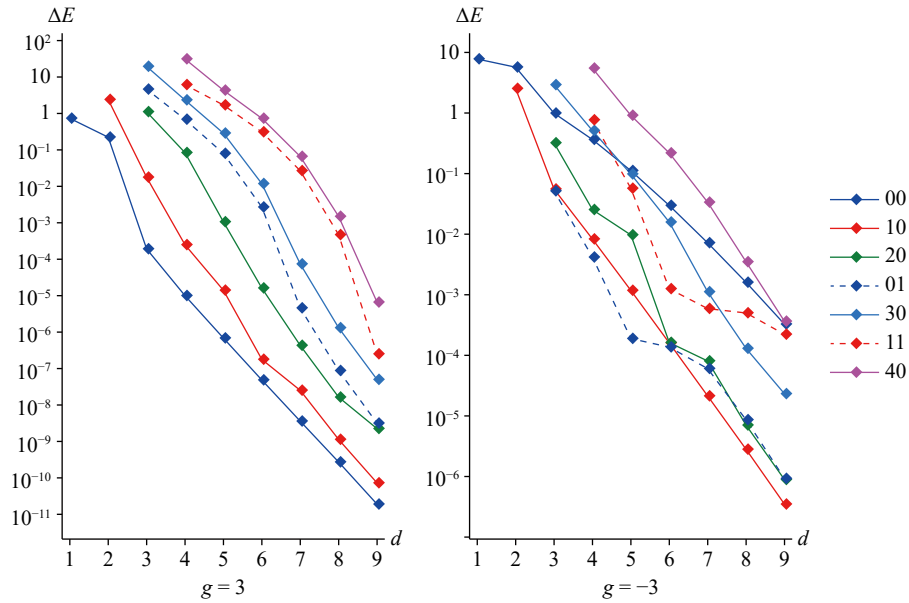


**Fig. 4** The convergence of the first few eigenenergies  $E_{ij}(d) - E_{ij}(d = 18)$ , with respect to the truncating degree  $d$  in the GCM basis.

The smooth continuation of the energy spectra, guaranteed by the Hellmann–Feynman theorem [91], is achieved through manual judgment and tracking the evolution of the eigenstate pattern. Two spectra degenerate at both the BE limit with  $E(0) = 7$  and the TG limit with  $E(+\infty) = 10$ . Their eigenenergies split slightly at finite  $g > 0$ . One of them,  $\Psi_{30}$ , follows a similar pattern of  $\Psi_{00}$ ,  $\Psi_{10}$  and  $\Psi_{20}$  in the radial direction but no longer maintains the  $SO(2)$  symmetry at the BE limit. In the axial direction, it gains one more node than  $\Psi_{20}$ . The other state,  $\Psi_{01}$ , has a finite sTG value  $E(-\infty) = 4$ , smoothly mapping the TG limit of  $\Psi_{00}$  in the sense of  $\frac{dE}{d(-g^{-1})}$  (as also exhibited by the Hellmann–Feynman theorem [59]), illustrating the TG/sTG mapping. Based on the TG limit of  $\Psi_{00}$ , it grows in density from the connection regions, gaining two nodes between them and the existing peaks in each sextant in the radial direction.

A similar pattern repeats for upper states: at the sTG limit, the spectrum  $\Psi_{ij}(j > 0)$  smoothly succeeds the TG limit of the predecessor spectrum  $\Psi_{i,j-1}$ , while the spectrum  $\Psi_{i0}$  grows from  $E_r = -\infty$ . The wave function  $\Psi_{ij}$  have  $i$  nodes in the axial direction and  $2j$  nodes in each sextant in the radial direction; its relative energy  $E_r$  is  $2i + 6j + 1$  at the BE and  $2i + 6j + 4$  at the TG limit, where  $j + 1$  states degenerate together. Their energies are slightly split at intermediate  $g$ , following the order that a state with higher  $j$  has a higher eigenenergy at  $g > 0$ , but a lower one at  $g < 0$ . This behavior is the 3-body extension of the Zel’dovich effect [92] and the pattern of energy spectra is consistent with Ref. [60].

By checking the computed weights of the polynomial terms in the GCM results, we can see that the wave function solutions are even at the BE limit and odd at

the TG limit. At these two limits, the results are exact, and the relative eigenenergy  $E_r$  equal to 1 plus the finite degree  $d_p$  of the polynomial  $p$  in the eigenstate, provided that  $d_p$  does not exceed the truncating degree  $d$  in the GCM basis. In other words, the results at the BE and TG limits with eigenenergy below  $d + 1$  are exact. For a  $d = 18$  basis, 15 energy spectra, in 8 levels, are fully below this upper bound (see Fig. 2). The energy spectra deviate noticeably from the regular pattern as  $E_r$  increases a few units beyond this upper bound.

### 3.2 Validations

To verify our results, first, we check the convergence of our eigenenergies by increasing the truncation degree  $d$  in our GCM basis. As shown in Fig. 4, the relative eigenenergy  $E_r$  monotonically decreases as  $d$  increases and exponentially converges as  $d + 1$  exceeds it. The value of the ground energy at an intermediate repulsive  $g > 0$  computed by a  $d = 3$  GCM basis (with 6 independent generating functions) is only  $\sim 10^{-4}$  higher than the converged value. Generally, the eigenenergies at  $g < 0$  converge more slowly, though still exponentially. As a comparison, Ref. [47] reports a discrepancy less than 1% for the ground energy at  $g > 0$ , obtained using  $\sim 1000$  configurations in the Hilbert space through the direct diagonalization method.

Then we compare the results with existing works. Our results of the ground eigenenergy at  $g > 0$  exactly match those received by the GCM-CPWF [53] in their decimal precision ( $10^{-3}$ ) and also have high consistency with other methods, while we have a tiny lower value of  $\sim 10^{-3}$  for the first excited eigenenergy. Additionally, as

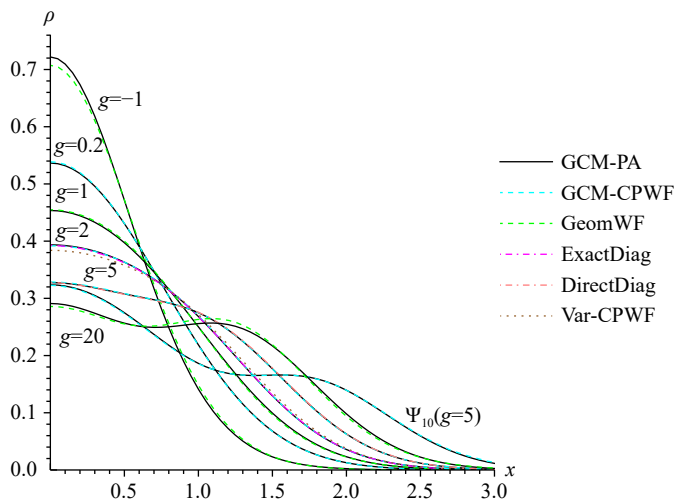


**Fig. 5** The one-particle densities obtained from our GCM-PA work, compared with other methods: GCM-CPWF [53], CPWF treating the parameter  $\beta$  variationally [52], geometric wave function [54], exact diagonalization [51] and direct diagonalization [47]. All states, except the otherwise noted  $\Psi_{10}(g=5)$ , are the ground state  $\Psi_{00}$ .

shown in Fig. 5, the single-particle density

$$\rho(x) = \int |\Psi_1(x, x_2, x_3)|^2 dx_2 dx_3 \quad (3.1)$$

of both the ground state and the first excited state at  $g > 0$  in our results precisely matches existing literature using other methods. Minor deviations are observed with the CPWF [52] and the geometric wave function [54], which may be attributed to the limitations inherent in their methods.

### 3.3 Discussion

In our reproduction of the GCM-CPWF [53], it deviates from our GCM-PA results above the second excited eigenenergies and fails to reveal the reported pattern of degenerating energy spectra [60]. Also, the interaction is restricted to  $g > 0$ . This is reasonable as its generating function is an adjustment of the CPWF function [52], which is a nice description of the ground state at  $g > 0$  but not tailored for the excited states or  $g < 0$  case of the system. Since our polynomial ansatz is free from such presuppositions on the shape of the wave function, the GCM-PA basis spans more sufficiently in the Hilbert space and offers a more flexible and fundamental way to obtain convergent eigenstates. Furthermore, while the GCM-CPWF relies on the Monte Carlo method for numerical integrations in the GCM kernels and restricts the number of generating functions to  $\sim 10$  due to the computational costs, the GCM-PA basis with analytical kernels can contain more functions to superpose, thereby enhancing accuracy.

Besides the advantages in calculation, the wave func-

tions expressed in the form of the polynomial ansatz reveal their regularity relatively easily. The GCM-PA may be flexibly adapted to other three-body systems with different symmetries, such as a pair of identical fermions with one different fermion ( $2+1$  fermions system). There is also potential to adapt this approach to solve variants of interaction forms.

The calculation of our GCM kernels for  $N=3$  is analytically solvable, while higher-dimensional integrations on the region  $x_1 < x_2 < \dots < x_N$  are not easily handled; additionally, the number of polynomials contained in the GCM basis increases significantly with the degree of freedom, showing the difficulties in directly adapting the PA to systems with more particles  $N \geq 4$ . Nevertheless, their potential presupposition functions may be guided by deeper investigations into the patterns in the  $N=3$  system obtained from our GCM-PA.

## 4 Conclusions

This paper studies the quantum system of three one-dimensional identical bosons with  $\delta$ -contact interaction in a harmonic trap. By analyzing its asymptotic behavior, we introduce a polynomial ansatz (PA) to describe the wave function and apply the generator coordinate method (GCM), with parameters set as the exponents in the polynomial terms, to obtain the solution at each specific interaction strength.

Using the GCM-PA approach, we obtained converged results of not only the ground states but also excited states with energy up to  $\sim 20\hbar\omega$ . The energy spectra and eigenstates exhibit periodic patterns, as shown in Figs. 2 and 3. The numerical results are consistent with existing literature, and the ground states of the BE (Bose–Einstein) and TG (Tonks–Girardeau) limits, along with some known properties of fermionization and TG/sTG (super-TG) mapping, are reproduced.

The main contribution of our work is the numerical results and patterns of excited eigenenergies and eigenstates without additional presuppositions across the entire range of interaction strengths  $-\infty < g < +\infty$ , which have not been extensively studied. Our method may be flexible to adapt to systems with different symmetries or forms of interaction and may act as a stepping stone for further studies.

**Declarations** The authors declare that they have no competing interests and there are no conflicts.

**Acknowledgements** We thank Luan-Hong Pei for helpful discussions. This work is supported by the National Key R&D Program of China (No. 2023YFA1606701). This work was supported in part by the National Natural Science Foundation of China under contract Nos. 12175042, 11890710, 11890714, 12047514, 12147101, and 12347106.

## References

1. I. Bloch, J. Dalibard, and W. Zwerger, Many-body physics with ultracold gases, *Rev. Mod. Phys.* 80(3), 885 (2008)
2. M. Lewenstein, A. Sanpera, and V. Ahufinger, *Ultracold Atoms in Optical Lattices: Simulating Quantum Many-Body Systems*, Oxford University Press, 2012
3. L. Sanchez-Palencia, *Disordered, ultracold quantum gases: Theoretical studies and experimental perspectives*, Ph. D. thesis, Université Paris Sud-Paris XI, 2011
4. M. A. García-March, B. Juliá-Díaz, G. E. Astrakharchik, Th. Busch, J. Boronat, and A. Polls, Quantum correlations and spatial localization in one-dimensional ultracold bosonic mixtures, *New J. Phys.* 16(10), 103004 (2014)
5. T. Sowiński and M. Á. García-March, One-dimensional mixtures of several ultracold atoms: A review, *Rep. Prog. Phys.* 82(10), 104401 (2019)
6. N. T. Zinner, Exploring the few- to many-body crossover using cold atoms in one dimension, in: 21st International Conference on Few-Body Problems in Physics, Vol. 113, EPJ Web of Conferences, EDP Sciences, 2016, p. 01002
7. M. A. Cazalilla, R. Citro, T. Giamarchi, E. Orignac, and M. Rigol, One dimensional bosons: From condensed matter systems to ultracold gases, *Rev. Mod. Phys.* 83(4), 1405 (2011)
8. C. H. Greene, P. Giannakeas, and J. Pérez-Ríos, Universal few-body physics and cluster formation, *Rev. Mod. Phys.* 89(3), 035006 (2017)
9. M. Girardeau, Relationship between systems of impenetrable bosons and fermions in one dimension, *J. Math. Phys.* 1(6), 516 (1960)
10. E. H. Lieb and W. Liniger, Exact analysis of an interacting Bose gas. I. The general solution and the ground state, *Phys. Rev.* 130(4), 1605 (1963)
11. E. H. Lieb, Exact analysis of an interacting Bose gas. II. The excitation spectrum, *Phys. Rev.* 130(4), 1616 (1963)
12. J. B. McGuire, Study of exactly soluble one-dimensional  $N$ -body problems, *J. Math. Phys.* 5(5), 622 (1964)
13. C. N. Yang, Some exact results for the many-body problem in one dimension with repulsive delta-function interaction, *Phys. Rev. Lett.* 19(23), 1312 (1967)
14. B. Sutherland, Further results for the many-body problem in one dimension, *Phys. Rev. Lett.* 20(3), 98 (1968)
15. F. Calogero, Solution of a three-body problem in one dimension, *J. Math. Phys.* 10(12), 2191 (1969)
16. B. Sutherland, Quantum many-body problem in one dimension: Ground state, *J. Math. Phys.* 12(2), 246 (1971)
17. X. W. Guan and P. He, New trends in quantum integrability: Recent experiments with ultracold atoms, *Rep. Prog. Phys.* 85(11), 114001 (2022)
18. X. W. Guan, M. T. Batchelor, and C. Lee, Fermi gases in one dimension: From Bethe ansatz to experiments, *Rev. Mod. Phys.* 85(4), 1633 (2013)
19. M. H. Anderson, J. R. Ensher, M. R. Matthews, C. E. Wieman, and E. A. Cornell, Observation of Bose-Einstein condensation in a dilute atomic vapor, *Science* 269(5221), 198 (1995)
20. C. Chin, R. Grimm, P. Julienne, and E. Tiesinga, Feshbach resonances in ultracold gases, *Rev. Mod. Phys.* 82(2), 1225 (2010)
21. M. Olshanii, Atomic scattering in the presence of an external confinement and a gas of impenetrable bosons, *Phys. Rev. Lett.* 81(5), 938 (1998)
22. M. Greiner, O. Mandel, T. Esslinger, T. W. Hänsch, and I. Bloch, Quantum phase transition from a superfluid to a Mott insulator in a gas of ultracold atoms, *Nature* 415(6867), 39 (2002)
23. S. L. Cornish, M. R. Tarbutt, and K. R. A. Hazzard, Quantum computation and quantum simulation with ultracold molecules, *Nat. Phys.* 20(5), 730 (2024)
24. J. K. Pachos and P. L. Knight, Quantum computation with a one-dimensional optical lattice, *Phys. Rev. Lett.* 91(10), 107902 (2003)
25. I. Bloch, J. Dalibard, and S. Nascimbene, Quantum simulations with ultracold quantum gases, *Nat. Phys.* 8(4), 267 (2012)
26. I. Bloch, Quantum simulations come of age, *Nat. Phys.* 14(12), 1159 (2018)
27. C. C. Chien, S. Peotta, and M. Di Ventra, Quantum transport in ultracold atoms, *Nat. Phys.* 11(12), 998 (2015)
28. S. I. Mistakidis, A. G. Volosniev, R. E. Barfknecht, T. Fogarty, Th. Busch, A. Foerster, P. Schmelcher, and N. T. Zinner, Few-body Bose gases in low dimensions — A laboratory for quantum dynamics, *Phys. Rep.* 1042, 1 (2023)
29. A. S. Dehkharghani, One-dimensional quantum systems - From few to many particles, arXiv: 1801.04993 (2018)
30. A. Rojo-Francàs, F. Isaule, and B. Juliá-Díaz, Few particles with an impurity in a one-dimensional harmonic trap, *Phys. Scr.* 99(4), 045408 (2024)
31. L. Tonks, The complete equation of state of one, two and three-dimensional gases of hard elastic spheres, *Phys. Rev.* 50(10), 955 (1936)
32. T. Nagamiya, Statistical mechanics of one-dimensional substances I, *Proc. Phys. Math. Soc. Jap. 3rd Ser.* 22(8), 705 (1940)
33. T. Cheon, and T. Shigehara, Fermion-boson duality of one-dimensional quantum particles with generalized contact interactions, *Phys. Rev. Lett.* 82(12), 2536 (1999)
34. M. D. Girardeau, E. M. Wright, and J. M. Triscari, Ground-state properties of a one-dimensional system of hard-core bosons in a harmonic trap, *Phys. Rev. A* 63(3), 033601 (2001)
35. B. Paredes, A. Widera, V. Murg, O. Mandel, S. Fölling, I. Cirac, G. V. Shlyapnikov, T. W. Hänsch, and I. Bloch, Tonks-Girardeau gas of ultracold atoms in an optical lattice, *Nature* 429(6989), 277 (2004)
36. T. Kinoshita, T. Wenger, and D. S. Weiss, Observation of a one-dimensional Tonks-Girardeau gas, *Science* 305(5687), 1125 (2004)
37. T. Kinoshita, T. Wenger, and D. S. Weiss, Local pair correlations in one-dimensional Bose gases, *Phys. Rev. Lett.* 95(19), 190406 (2005)
38. L. Yang, S. S. Alam, and H. Pu, Generalized



- Bose–Fermi mapping and strong coupling ansatz wavefunction for one dimensional strongly interacting spinor quantum gases, *J. Phys. A Math. Theor.* 55(46), 464005 (2022)
39. G. E. Astrakharchik, J. Boronat, J. Casulleras, and S. Giorgini, Beyond the Tonks–Girardeau gas: Strongly correlated regime in quasi-one-dimensional Bose gases, *Phys. Rev. Lett.* 95(19), 190407 (2005)
  40. M. T. Batchelor, M. Bortz, X. W. Guan, and N. Oelkers, Evidence for the super Tonks–Girardeau gas, *J. Stat. Mech.* 2005(10), L10001 (2005)
  41. E. Haller, M. Gustavsson, M. J. Mark, J. G. Danzl, R. Hart, G. Pupillo, and H. C. Nägerl, Realization of an excited, strongly correlated quantum gas phase, *Science* 325(5945), 1224 (2009)
  42. S. Chen, L. Guan, X. Yin, Y. Hao, and X. W. Guan, Transition from a Tonks–Girardeau gas to a super-Tonks–Girardeau gas as an exact many-body dynamics problem, *Phys. Rev. A* 81(3), 031609 (2010)
  43. Th. Busch, B. G. Englert, K. Rzażewski, and M. Wilkens, Two cold atoms in a harmonic trap, *Found. Phys.* 28(4), 549 (1998)
  44. B. B. Wei, Two one-dimensional interacting particles in a harmonic trap, *Int. J. Mod. Phys. B* 23(18), 3709 (2009)
  45. P. Shea, B. P. van Zyl, and R. K. Bhaduri, The two-body problem of ultra-cold atoms in a harmonic trap, *Am. J. Phys.* 77(6), 511 (2009)
  46. A. Farrell and B. P. van Zyl, Universality of the energy spectrum for two interacting harmonically trapped ultra-cold atoms in one and two dimensions, *J. Phys. A Math. Theor.* 43(1), 015302 (2010)
  47. A. Rojo-Francàs, F. Isaule, and B. Juliá-Díaz, Direct diagonalization method for a few particles trapped in harmonic potentials, *Phys. Rev. A* 105(6), 063326 (2022)
  48. P. Kościuk, A. Kuroś, A. Pieprzycki, and T. Sowiński, Pair-correlation ansatz for the ground state of interacting bosons in an arbitrary one-dimensional potential, *Sci. Rep.* 11(1), 13168 (2021)
  49. P. Kościuk, M. Płodzień, and T. Sowiński, Variational approach for interacting ultra-cold atoms in arbitrary one-dimensional confinement, *Europhys. Lett.* 123(3), 36001 (2018)
  50. S. Zöllner, H. D. Meyer, and P. Schmelcher, Ultracold few-boson systems in a double-well trap, *Phys. Rev. A* 74(5), 053612 (2006)
  51. F. Deuretzbacher, K. Bongs, K. Sengstock, and D. Pfannkuche, Evolution from a Bose–Einstein condensate to a Tonks–Girardeau gas: An exact diagonalization study, *Phys. Rev. A* 75(1), 013614 (2007)
  52. I. Brouzos and P. Schmelcher, Construction of analytical many-body wave functions for correlated bosons in a harmonic trap, *Phys. Rev. Lett.* 108(4), 045301 (2012)
  53. J. A. Sun, G. J. Guo, B. Zhou, and Y. G. Ma, Generator coordinate method for 1D contacting bosons in harmonic trap, *J. Phys. At. Mol. Opt. Phys.* 56(21), 215301 (2023)
  54. B. Wilson, A. Foerster, C. C. N. Kuhn, I. Roditi, and D. Rubeni, A geometric wave function for a few interacting bosons in a harmonic trap, *Phys. Lett. A* 378(16–17), 1065 (2014)
  55. T. Grining, M. Tomza, M. Lesiuk, M. Przybytek, M. Musiał, P. Massignan, M. Lewenstein, and R. Moszynski, Many interacting fermions in a one-dimensional harmonic trap: A quantum-chemical treatment, *New J. Phys.* 17(11), 115001 (2015)
  56. E. J. Lindgren, J. Rotureau, C. Forssén, A. G. Volosniev, and N. T. Zinner, Fermionization of two-component few-fermion systems in a one-dimensional harmonic trap, *New J. Phys.* 16(6), 063003 (2014)
  57. B. Schmidt and M. Fleischhauer, Exact numerical simulations of a one-dimensional trapped Bose gas, *Phys. Rev. A* 75(2), 021601 (2007)
  58. G. E. Astrakharchik and S. Giorgini, Correlation functions and momentum distribution of one-dimensional Bose systems, *Phys. Rev. A* 68(3), 031602 (2003)
  59. E. K. Laird, Z. Y. Shi, M. M. Parish, and J. Levinsen,  $SU(N)$  fermions in a one-dimensional harmonic trap, *Phys. Rev. A* 96(3), 032701 (2017)
  60. N. L. Harshman, Symmetries of three harmonically trapped particles in one dimension, *Phys. Rev. A* 86(5), 052122 (2012)
  61. N. L. Harshman, Spectroscopy for a few atoms harmonically trapped in one dimension, *Phys. Rev. A* 89(3), 033633 (2014)
  62. S. Zöllner, H. D. Meyer, and P. Schmelcher, Excitations of few-boson systems in one-dimensional harmonic and double wells, *Phys. Rev. A* 75(4), 043608 (2007)
  63. X. J. Liu, H. Hu, and P. D. Drummond, Three attractively interacting fermions in a harmonic trap: Exact solution, ferromagnetism, and high-temperature thermodynamics, *Phys. Rev. A* 82(2), 023619 (2010)
  64. P. D’Amico and M. Rontani, Three interacting atoms in a one-dimensional trap: A benchmark system for computational approaches, *J. Phys. At. Mol. Opt. Phys.* 47(6), 065303 (2014)
  65. N. T. Zinner, A. G. Volosniev, D. V. Fedorov, A. S. Jensen, and M. Valiente, Fractional energy states of strongly interacting bosons in one dimension, *Europhys. Lett.* 107(6), 60003 (2014)
  66. N. L. Harshman and A. C. Knapp, Anyons from three-body hard-core interactions in one dimension, *Ann. Phys.* 412, 168003 (2020)
  67. C. W. Wong, Generator-coordinate methods in nuclear physics, *Phys. Rep.* 15(5), 283 (1975)
  68. J. Broeckhove and E. Deumens, A mathematical foundation for discretisation techniques in the generator coordinate method, *Z. Phys. A* 292(3), 243 (1979)
  69. J. R. Mohallem, A further study on the discretisation of the Griffin–Hill–Wheeler equation, *Z. Phys. D* 3(4), 339 (1986)
  70. P. G. Reinhard and K. Goeke, The generator coordinate method and quantised collective motion in nuclear systems, *Rep. Prog. Phys.* 50(1), 1 (1987)
  71. P. Ring and P. Schuck, *The Nuclear Many-Body Problem*, Springer, 2004
  72. D. L. Hill and J. A. Wheeler, Nuclear constitution and the interpretation of fission phenomena, *Phys. Rev.* 89(5), 1102 (1953)
  73. J. J. Griffin and J. A. Wheeler, Collective motions in nuclei by the method of generator coordinates, *Phys.*

- Rev.* 108(2), 311 (1957)
74. T. Ichikawa and N. Itagaki, Optimization of basis functions for multiconfiguration mixing using the replica exchange Monte Carlo method and its application to  $^{12}\text{C}$ , *Phys. Rev. C* 105(2), 024314 (2022)
  75. N. Hizawa, K. Hagino, and K. Yoshida, Applications of the dynamical generator coordinate method to quadrupole excitations, *Phys. Rev. C* 105(6), 064302 (2022)
  76. X. Zhang, W. Lin, J. M. Yao, C. F. Jiao, A. M. Romero, T. R. Rodríguez, and H. Hergert, Optimization of the generator coordinate method with machine-learning techniques for nuclear spectra and neutrinoless double- $\beta$  decay: Ridge regression for nuclei with axial deformation, *Phys. Rev. C* 107(2), 024304 (2023)
  77. Y. Huang, X. Y. Wu, X. L. Tu, Z. P. Li, Y. Kuang, J. T. Zhang, and Z. H. Li, Matter density distributions and radii from small-angle differential cross sections of proton-nucleus elastic scattering at 0.8 GeV, *Phys. Rev. C* 108(5), 054610 (2023)
  78. T. Myo and H. Takemoto, Resonances and scattering in microscopic cluster models with the complex-scaled generator coordinate method, *Phys. Rev. C* 107(6), 064308 (2023)
  79. B. Zhou, Y. Funaki, H. Horiuchi, Y. G. Ma, G. Röpke, P. Schuck, A. Tohsaki, and T. Yamada, The  $5\alpha$  condensate state in  $^{20}\text{Ne}$ , *Nat. Commun.* 14(1), 8206 (2023)
  80. Y. Y. Cao, D. Y. Tao, and B. Zhou, Microscopic cluster study of the  $^{10}\text{Be}$  nucleus, *Nucl. Phys. Rev.* 41(1), 148 (2024)
  81. B. Li, D. Vretenar, T. Nikšić, J. Zhao, P. W. Zhao, and J. Meng, Generalized time-dependent generator coordinate method for induced fission dynamics, *Front. Phys.* (Beijing) 19(4), 44201 (2024)
  82. P. Descouvemont and M. Dufour, Equivalence between two- and three-cluster models: Application to the  $^{15}\text{C}$  and  $^{15}\text{F}$  nuclei, *Phys. Rev. C* 109(3), 034303 (2024)
  83. Y. Beaujeault-Taudière and D. Lacroix, Solving the Lipkin model using quantum computers with two qubits only with a hybrid quantum-classical technique based on the generator coordinate method, *Phys. Rev. C* 109(2), 024327 (2024)
  84. A. Porro, T. Duguet, J. P. Ebran, M. Frosini, R. Roth, and V. Somá, Ab initio description of monopole resonances in light- and medium-mass nuclei: I. technical aspects and uncertainties of ab initio PGCM calculations, *Eur. Phys. J. A* 60(6), 133 (2024)
  85. D. M. Brink and A. Weiguny, The generator coordinate theory of collective motion, *Nucl. Phys. A.* 120(1), 59 (1968)
  86. K. N. Hsu, The generator coordinate method and nuclear collective motions, *Sci. Sin.* XVII(5), 639 (1974)
  87. R. Shankar, Principles of Quantum Mechanics, New York: Plenum Press, 2nd Ed., 1994
  88. H. Lütkepohl, Handbook of Matrices, John Wiley & Sons, 1997
  89. H. Bethe and R. Peierls, Quantum theory of the dipton, *Proc. R. Soc. Lond. A* 148(863), 146 (1935)
  90. F. W. J. Olver, D. W. Lozier, R. F. Boisvert, and C. W. Clark, NI Mathematical Functions, Cambridge University Press, 2010
  91. R. P. Feynman, Forces in molecules, *Phys. Rev.* 56(4), 340 (1939)
  92. A. Farrell, Z. MacDonald, and B. P. van Zyl, The Zel'dovich effect in harmonically trapped, ultracold quantum gases, *J. Phys. A Math. Theor.* 45(4), 045303 (2012)